

# On some inverse problems in nuclear physics

B.Z. Belashev<sup>1)</sup> and M.K. Suleymanov<sup>2,3)</sup>

<sup>1)</sup> Institute of Geology, Karelian Research Centre, RAS, Petrozavodsk, Russia

<sup>2)</sup> LHE JINR, Dubna, Moscow region, Russia

<sup>3)</sup> NPI ASCR, Rez near Prague, Czech Republic

## Abstract

Some inverse problems in high-energy physics, neutron diffraction and NMR spectroscopy are discussed. To solve them, the Fourier integrated transformation method and the Maximum Entropy Technique (MENT) were used. The integrated images of experimental distributions are shown to be informative when determining the space-time parameters of a particle generation zone and when analysing blurred spectra. The efficiency of the above methods was checked by comparing relevant results with the results obtained independently.

An inverse problem arises where the information required can not be obtained through direct measurements. The majority of inverse problems in nuclear physics is connected to interpretation of experimental data on scattering high-energy particles on targets. The scattering pattern is used to determine the structure of colliding particles, interaction potential and the dynamics of processes occurring upon collision. In some cases, a nucleus or a particle is understood as a probe with known magnetic moment, wave length and energy level system. Its interaction with a substance and a field is used to assess the concentration of the substance, the characteristics of the medium or the configuration of the field. Such inverse tasks are typical of NMR and NGR spectroscopy, neutron diffraction, activating analysis, emitted tomography and other applications of nuclear physics.

In this paper, some inverse problems arising in experiments in high-energy physics are discussed [1, 2, 3, 4, 5]. To solve them, filtration methods are used. Experimental data are subjected to Fourier transformation to obtain a result without a substantial use of a priori restrictions [3, 6]. This property is especially important when selecting models of processes in cases when the experimental distributions are compatible with several models and the application of approximation methods is ineffective.

One question, which arises when solving an inverse task, is whether the results obtained are proven. This question can be answered by comparing the results obtained by independent methods. To illustrate such a comparison, diffusion spectra were used as an example, their resolution being increased instrumentally and a posteriori through the Maximum Entropy Technique (ENT) [7, 8, 9].

The goal of our study was to show that the same type of mathematical and algorithmic approaches, based on integrated transformations, can be used to solve some inverse tasks in nuclear physics.

## SPACE-TIME CHARACTERISTICS OF THE MULTIPLE BIRTH OF PARTICLES

Using Podgoretsky and Kopylov's approach, light can be thrown on the space-time characteristics of the multiple birth of particles by studying correlations of identical particles with close 4-impulses [1]. The probability  $W(q_0, \vec{q})$  of detecting two identical particles

with 4-impulses  $P_1 = \{\varepsilon_1, \vec{p}_1\}$  and  $P_2 = \{\varepsilon_2, \vec{p}_2\}$ , emitted by two point sources with the coordinates  $\{t_1, \vec{r}_1\}$  and  $\{t_2, \vec{r}_2\}$ , is expressed by the formula:

$$W(q_0, \vec{q}) = 1 + \frac{\cos[\vec{q}(\vec{r}_1 - \vec{r}_2) - q_0(t_1 - t_2)]}{1 + (q_0\tau)^2} \quad (1)$$

where  $\vec{q} = \vec{p}_1 - \vec{p}_2$ ,  $q_0 = \varepsilon_1 - \varepsilon_2$ ,  $\tau$  is the lifetime of the sources. For identical particles of identical energy  $q_0 = 0$ , a relationship (1) is determined by a spatial variable  $\vec{R} = \vec{r}_1 - \vec{r}_2$ :

$$W(\vec{q}) = 1 + \cos(\vec{q}\vec{R}). \quad (2)$$

The above formulas hold for identical particles that obey Boze-Einstein statistics, e.g. the  $\pi$ -mesons of large impulses. Let us assume that  $f(\vec{R})$  is the normalized spatial distribution of the sources of particles on the  $\vec{R}$ . Then the formula (2) for the probability  $W(\vec{q})$  has the form:

$$W(\vec{q}) = 1 + \int f(\vec{R}) \cos(\vec{q}\vec{R}) d\vec{R}. \quad (3)$$

In this case  $f(\vec{R}) = f(-\vec{R})$ , because two identical particles are indexed by two equivalent methods. The function  $W(\vec{q})$  does not depend on the sign  $\vec{R}$  and the integrated addend in (3) is the Fourier image  $F(\vec{q})$  of the function  $f(\vec{R})$

$$W(\vec{q}) = 1 + F(\vec{q}). \quad (4)$$

Thus, the experimental relationship  $W(\vec{q})$  is used to obtain the Fourier image of the distribution function  $f(\vec{R})$

$$F(\vec{q}) = W(\vec{q}) - 1 \quad (5)$$

and to use it, in turn, to calculate the distribution function  $f(\vec{R})$  by inverse Fourier transformation.

In collisions of identical particles, experimental data can directly provide information on the distribution density of the sources  $\rho(\vec{r})$  in the generation field, provided the sources of the particles are independent [2]. The Fourier image  $G(\vec{q})$  of the function  $\rho(\vec{r})$  is calculated using the formula

$$G(\vec{q}) = \sqrt{W(\vec{q}) - 1} \quad (6)$$

and the function  $\rho(\vec{r})$  is estimated by its inverse Fourier transformation. The three-dimensional function  $\rho(\vec{r})$  can be represented for convenience as cutting of the generation zone by a system of parallel planes or a projection of the generation zone to a plane perpendicular to the preset direction. The condition  $\rho(\vec{r}) \geq 0$  restricts experimental distributions to a certain class of functions. Such a restriction is automatically removed if the distribution of the sources is reconstructed by its Fourier image using ENT [10].

A similar technique of selecting identical particles with  $\vec{q} = 0$  to estimate the distribution function of the sources on the variable  $t = t_1 - t_2$  is impossible as it results in the value  $q_0 = 0$ , which follows from a condition relating the masses, energies and impulses of identical particles. When discussing a general case, we will not restrict the  $q_0$  value.

Let us introduce the normalized distribution function  $f_1(\vec{R}, t, \tau)$  and re-write the formula (1), considering a trigonometrical identity:

$$\cos(\vec{q}\vec{R} - q_0t) = \cos(\vec{q}\vec{R}) \cos(q_0t) + \sin(\vec{q}\vec{R}) \sin(q_0t) \quad (7)$$

as

$$W(q_0, \vec{q}) = 1 + \int f_1(\vec{R}, t, \tau) \frac{\cos(\vec{q}\vec{R}) \cos(q_0t) d\vec{R} dt d\tau}{1 + (q_0\tau)^2} + \int f_1(\vec{R}, t, \tau) \frac{\sin(\vec{q}\vec{R}) \sin(q_0t) d\vec{R} dt d\tau}{1 + (q_0\tau)^2}. \quad (8)$$

The second integral addend in the formula (8) is equal to zero because the methods of indexing of a particle in a pair are indential, the function  $f_1(\vec{R}, t, \tau)$  is even and the function of a sine on the variables  $\vec{R}$  and  $t$  is odd.

In the assumption about the independence of spatial, temporal and relaxation distributions, described accordingly by the normalized functions  $f(\vec{R})$ ,  $\chi(t)$  and  $\varphi(\tau)$ , expressed by the condition

$$f_1(\vec{R}, t, \tau) = f(\vec{R}) \cdot \chi(t) \cdot \varphi(\tau) \quad (9)$$

formula (8) is re-written as

$$W(q_0, \vec{q}) = 1 + \int f(\vec{R}) \cos(\vec{q}\vec{R}) d\vec{R} \int \chi(t) \cos(q_0t) dt \int \frac{\varphi(\tau) d\tau}{1 + (q_0\tau)^2}. \quad (10)$$

The first two integrated co-multipliers in (10) represent the Fourier images  $F(\vec{q})$  and  $X(q_0)$  of the normalized spatial  $f(\vec{R})$  and temporal  $\chi(t)$  distributions. The third integrated multiplier does not depend on the magnitude of  $q_0$ , which follows from the condition of normalizing of the function  $\varphi(\tau)$

$$\int_0^\infty \varphi(\tau) d\tau = \int_0^\infty \varphi(q_0\tau) d(q_0\tau) = 1. \quad (11)$$

and can be written as constant  $C = \int_0^\infty \frac{\varphi(q_0\tau) d(q_0\tau)}{1 + (q_0\tau)^2} > 0$ . The formula (10) then has the form

$$W(q_0, \vec{q}) = 1 + CF(\vec{q})X(q_0) \quad (12)$$

can be used to estimate the function  $CX(q_0)$  from the experimental relations  $W(q_0, \vec{q})$  and  $W(0, \vec{q})$

$$CX(q_0) = \frac{W(q_0, \vec{q}) - 1}{F(\vec{q})} = \frac{W(q_0, \vec{q}) - 1}{W(0, \vec{q}) - 1}. \quad (13)$$

The distribution function of the sources  $\chi(t)$  is determined by inverse Fourier transformation of the function  $CX(q_0)$  and subsequent normalization by unit.

In this problem, the integrated images of spatial and temporal distribution of the sources of particles are present in the data obtained by the interference experiment, and can be revealed if the data are represented in a special manner. In some cases, an artificial transition from experimental distributions to their integrated images and nonlinear operations with them can be useful. There is a class of such operations that can be done in the case of inverse transition to obtain more informative estimates of data than in initial distributions [11].

## RETRIEVAL OF BARION RESONANCES IN EFFECTIVE MASS SPECTRA

The aim of our study was to investigate two-particle correlations of the reaction products of multiple birth at high energies that are observed in the distributions of pairs of secondary particles on the effective mass  $M_{eff}$  and provide information on compound systems or resonances formed during particle generation. Of interest for the study of collision dynamics are  $\Delta$ -isobars, barion resonances that form a connected short-lived system from a nucleon and a  $\pi$ -meson. This interest is due to the fact that the birth of such resonances on nuclei upon collision of hadrons with the nuclei at low energies can provide the main channel for elastic scattering. Isobars can give information about interaction with other fragments of the nucleus and enable us to experimentally study the colour degrees of freedom.

The purpose of the study of the effective mass spectra ( $\pi^\pm p$ ) pairs in  $\pi^- p$  and  $\pi^{-12}C$  interactions at  $P_{\pi^-} = 40 GeV/c$  is to determine the structure of the spectra and to relate the birth of barion resonances and a special case of the multiple generation of hadrons, such as birth of cumulative particles in  $\pi^{-12}C$  interactions [4].

The spectra of the effective masses of pairs were plotted on the basis of non-elastic 11688  $\pi^- p$  and 8642  $\pi^{-12}C$  interactions obtained by analysis of stereo photos taken by a two-metre propane camera of LHE JINR irradiated by a bundle of  $\pi$ -mesons from the Serpukhov accelerator [12]. The effective mass of pairs was calculated using the formula:

$$M_{eff} = \sqrt{m_p^2 + m_\pi^2 + 2(E_p E_\pi - p_p p_\pi \cos \theta)} \quad (14)$$

using the masses of proton and  $\pi$ -meson  $m_p$  and  $m_\pi$  their total energies  $E_p$  and  $E_\pi$  the absolute values of impulses  $p_p$  and  $p_\pi$  and an angle  $\theta$  between impulses (in a laboratory system). The impulse of the protons selected varied from 140 to 700 MeV/s.

To establish a relation between the birth of  $\Delta$  isobars and the cumulative irradiation of  $\pi$ -mesons in interactions, two schemes of selection of secondary  $\pi$ -mesons in the event were used. In the first scheme, all  $\pi$ -mesons of the event were considered. In the second scheme,  $\pi$ -meson with a maximum cumulative order value in the event was excluded. The cumulative order of  $\pi$ -meson was determined in accordance with the formula  $n_c = \frac{E - p_{||}}{m_N}$  through total energy  $E$ , longitudinal impulse  $p_{||}$  of  $\pi$ -meson and the mass of the nucleon  $m_N$ . The structure of the effective mass spectra  $\pi^\pm p$  pairs was analysed using two data processing methods based on Fourier transformation. In the former method, we revealed the periodicities of the dependence of the module of the Fourier image of a symmetric spectrum on angular frequency. These, in turn, were used to determine the positions of structural components corresponding to resonance masses [3]. The results obtained by this method are shown in Figure 1. The positions of the specified characteristics of the spectra are shown by arrows, position errors by segments above the arrows and the value of the mass of known resonances by a number.

In the latter method, the idea to control the widths of the components of the effective mass spectrum was used [6]. The widths of the components in the estimation of the spectrum were diminished by multiplying the Fourier image of the spectrum by an exponential function. Upon inverse Fourier transformation of such an image, we the resultant estimate had a higher resolution than the initial spectrum and exhibited some characteristics that could be compared in effective mass to barion resonances [4].

The results obtained by this method are presented in Figure 2 which shows experimental distributions  $\frac{dN(M_{eff})}{dM_{eff}}$  and calculated estimates of  $f(M_{eff})$  corresponding to the pairs  $\pi^\pm p$  in the former scheme of selection of  $\pi$ -mesons of the event (a and b), and  $\pi^\pm p$  pairs in the latter scheme of selection (c and d). The main peak of the structures detected corresponds to a mass of 1.232 MeV/c<sup>2</sup> and additional peak corresponds to mass 1.650 MeV/c<sup>2</sup>. When cumulative  $\pi$ -mesons were eliminated, the estimates of the effective mass spectrum declined in a uniform manner by ca. 30% without changing the form.

The characteristics obtained in the effective mass spectra of  $\pi^\pm p$  pairs were compared to  $\Delta^{+0+}(1.232)$ ,  $\Delta^{+0+}(1.650)$ ,  $\Delta^{+0+}(1.670)$ ,  $\Delta^{+0+}(1.910)$  isobars in  $\pi^- p$  interactions and to  $\Delta^{+0+}(1.232)$ ,  $\Delta^{+0+}(1.650)$  isobars in  $\pi^{-12}C$  interactions. Analysis of the average multiplicity of  $\pi^+$  and  $\pi^-$ -mesons in  $\pi^{-12}C$  interactions at  $P_{\pi^-} = 40$  GeV/c, made with regard for the background of the spectra has shown that elimination of any  $\pi^-$  meson in the event decreases by about 30% in the distributions  $\frac{dN(M_{eff})}{dM_{eff}}$ . This result is believed to show that the generation of cumulative  $\pi$ -mesons and the birth of barion resonances are two independent processes.

## RAPIDITY-BASED PARTICLE DISTRIBUTION STRUCTURE

According to modern concepts of interaction between high-energy hadrons and nucleons and nuclei, secondary particles dominantly arise during the hadron transformation of fast quark parton into a jet of particles [13]. It is convenient to study this jet hadron transformation, seen in short-range correlations of interaction products, in the rapidity-based distributions of reaction products, observing the grouping of particles relative to several characteristic rapidities.

Rapidity is determine as  $y = (1/2) \ln((E + p_{||})/(E - p_{||}))$  where  $E$  and  $p_{||}$  are energy and the longitudinal impulse of a secondary particle.

Rapidity-based distributions are typically plotted as smooth curves without visible characteristics, which makes it difficult to select jets. To detect the characteristic rapidities of the multiple generation of  $\pi^\pm$ -mesons in  $\pi^- p$  and  $\pi^{-12}C$  reactions at  $P_{\pi^-} = 40$  GeV/c the method, used earlier to decrease the widths of distribution components, was applied [7].

Input data and the results of the application of this method are shown in Figure 3. The rapidity-based distributions of  $\pi^\pm$ -mesons in these reactions (a and b) are highly blurred, but their contrasting estimations (c and d) are structurally complex. In  $\pi^- p$  interaction, the estimate of rapidity-based distribution of  $\pi^+$ -mesons is a doublet with peaks  $y \approx 1.4$  and  $y \approx 2.8$ . For  $\pi^-$ -mesons, it consist of three peaks with  $y \approx 1.2$ ,  $y \approx 2.8$ ,  $y \approx 4.7$ . The estimates of rapidity-based distribution in  $\pi^{-12}C$  interactions for  $\pi^+$ -mesons contains three peaks with rapidities  $y \approx 1.4$ ,  $y \approx 2.8$ ,  $y \approx 3.3$  and three peaks with rapidities  $y \approx 0.9$ ,  $y \approx 2.5$ ,  $y \approx 4.4$  for  $\pi^-$ -mesons with a highly diffused second peak in the rapidity interval of 1.8-3.2.

The results obtained can be used to compare the characteristic rapidities of secondary  $\pi$ -mesons over the ranges 1.0–1.6; 1.8–3.2; 4.0–4.4 to the areas of fragmentation of a target, a colliding  $\pi$ -meson. The number and values of the characteristic rapidities of the process depend on the mass of the target and the charges of secondary  $\pi$ -mesons.

#### INCREASING THE INFORMATIVE CAPACITY OF SPECTRA BY MENT

A solution can be increased by diffusive spectra by the MENT. To increase the solution of experimental spectra, a variant of ENT with trial diffusion functions is used [7]. This variant is similar to Fourier method for regulating distribution widths, but has the best solution and stability to the noise [11].

In this study, MENT was used to reconstruct the inner structure of diffusive neutron diagrams and the NMR spectra of solid state. These spectra typically provide a tool for recording spectra that differ in resolution. This allows to compare the results obtained by processing the original diffuse low-resolution spectra with those obtained by recording high-resolution spectra and to find out whether diffuse spectra can be processed.

Neutron diffraction is an effective tool for the structural study of a substance due to various properties of a neutron and the comparability of its wave lengths and energies of neutrons to interatomic distances and excitation energies in solid and liquid states.

A convenient scheme of neutron diffraction, compatible with impulse reactors of neutrons, is the reflection of neutrons from an atomic plane at a constant angle with decomposition of reflection intensity in a spectrum on the wave length of neutrons or the flight time by neutrons of the defined base. When developing this technique, Fourier diffraction was accomplished with the help of a scheme of Fourier breakers of a beam on impulse reactors of neutrons. Neutron Fourier diffraction is characterized by a high spectral solution and by smaller level of a hum.

Fig. 4 shows neutron diagram of powder  $YBa_2(Cu, Fe)_3O_{63}Y_{12}$  registered with usual solution by a time of flight diffractometer (a) and neutron diagram of this sample measured on the IFR-2 reactor (LNF JINR Dubna) with high solution by Fourier diffractometer (b) [8]. Outcome of treatment of diagram (a) by the MENT: estimation and its touch diagram are gave on (c).

The comparison of these graphs suggests the similarity of structures represented by the MENT touch diagram and Fourier diagram.

NMR spectra provide important chemical, biophysical and medical information.

Magnetic resonance is characteristic of nuclei with a spin differing from zero placed in a magnetic field. It is observed as the precession of the magnetic moments of the nucleus in a magnetic field. The macroscopic vector of magnetization can be recorded during the interaction of moments with electromagnetic radiation containing frequency components near Larmor frequency  $\omega_0$  or under the influence of fast changes in the orientation of an external magnetic field. For this purpose, in addition to a static magnetic field, a radio frequency field with Larmor frequency  $\omega_0$  is applied perpendicularly to direction of static field or several types of RF-impulses (called  $\pi/2$ ,  $\pi$ ,  $3\pi/2$  and  $2\pi$  in accordance with the angle of turn of the magnetization vector in a rotating coordinate system) are used to initiate transition processes in a system of nuclear spins. A signal of free collapse of induction after the cessation of the action of  $\pi/2$  of impulse can be used, as a result of inverse transformation of Fourier, to obtain data on the characteristic frequencies of a system of nuclear spins as well as spin-lattice and spin-spin relaxation times.

NMR spectroscopy can conveniently be applied to liquids the spectra of which are represented by narrow spectral lines. The NMR spectra of solids, recorded by the forced precession method, are, on the contrary, diffuse and are hard to interpret. The reason for that is that the averaging of dipole-dipole spin-spin interaction is less efficient than in liquids. Artificial averaging became possible after using special sequences of  $\pi/2$  and  $\pi$  impulses [9]. The NMR spectra of solids then became similar to those of liquids.

Applying MENT to a low-resolution NMR, we can compare the estimate of the spectrum obtained with a high-resolution NMR spectrum. In this example, our purpose was to check up the ability of the MENT algorithm for the diffuse spectra of solids that have a constant noise level.

Figure 5 shows the NMR spectrum  $^{13}\text{C}$  of adamantane, an organic compound (a) recorded by the forced precession method (curve 1) and with the help  $\pi/2$ ,  $\pi$  sequences of impulses (curve 2) [9]. Also shown in the figure is a MENT estimate (curve 3) with its touch diagram (curve 4) (b) obtained by processing the diffuse NMR spectrum.

Characteristic of a processed spectrum is its arbitrary position on the ordinate axis, i. e. the lack of information on the constant component of hum noise. It is usually difficult to process and interpret such spectrum. Indeed, the touch diagram of the MENT estimate of this spectrum shows a series of peaks not of which have a background origin. However, there are typically two intensive peaks that reflect the true structure of the high-resolution NMR spectrum recorded.

This example shows that the hum noise of a diffusion spectrum should be accurately estimated to draw correct conclusions about its structure. It also shows that the position of the most intensive components of a diffusion spectrum can be determined even though there is no information on the constant constituent of hum noise.

#### Conclusions:

1. Based on the interference approach, a method for reconstruction of the space-time characteristics of a particle generation zone in collisions of high-energy particles is proposed. This method can be employed to determine the density functions of the space-time distributions of the sources of particles from the experimental distribution of pairs of secondary identical particles with respect to a difference in their impulses and energies, thus solving an inverse problem. The statistical provision of modern experiments of high-energy physics favours the application of this method.

2. The application of the methods of Fourier analysis of diffusion spectra to search for barion resonances and characteristic rapidities in the reactions of  $\pi^-p$  and  $\pi^-^{12}\text{C}$  interactions at  $P_{\pi^-} = 40 \text{ GeV}/c$  has made it possible to elucidate the structural characteristics of experimental distributions and to compare them with known  $\Delta$  isobars and zones of fragmentation of reaction products in the rapidity space. The results obtained by analysing the spectra of the effective masses of pairs using various schemes of selection of  $\pi$ -mesons in an event show that the formation of  $\Delta$  isobars and the emission of cumulative  $\pi$ -mesons are independent processes. This approach can be used to search for various resonances, multi-quark systems, exotic mesons and purely glue states [13].

3. In inverse problems arising in applied nuclear physics in neutron diffraction and NMR, MENT-based methods of analysis of diffuse spectra gave results comparable to those obtained by high-resolution instrumental methods. A high informative capacity of the MENT methods was supported by processing simple and complex spectra in the absence of data on the constant constituent of hum noise.

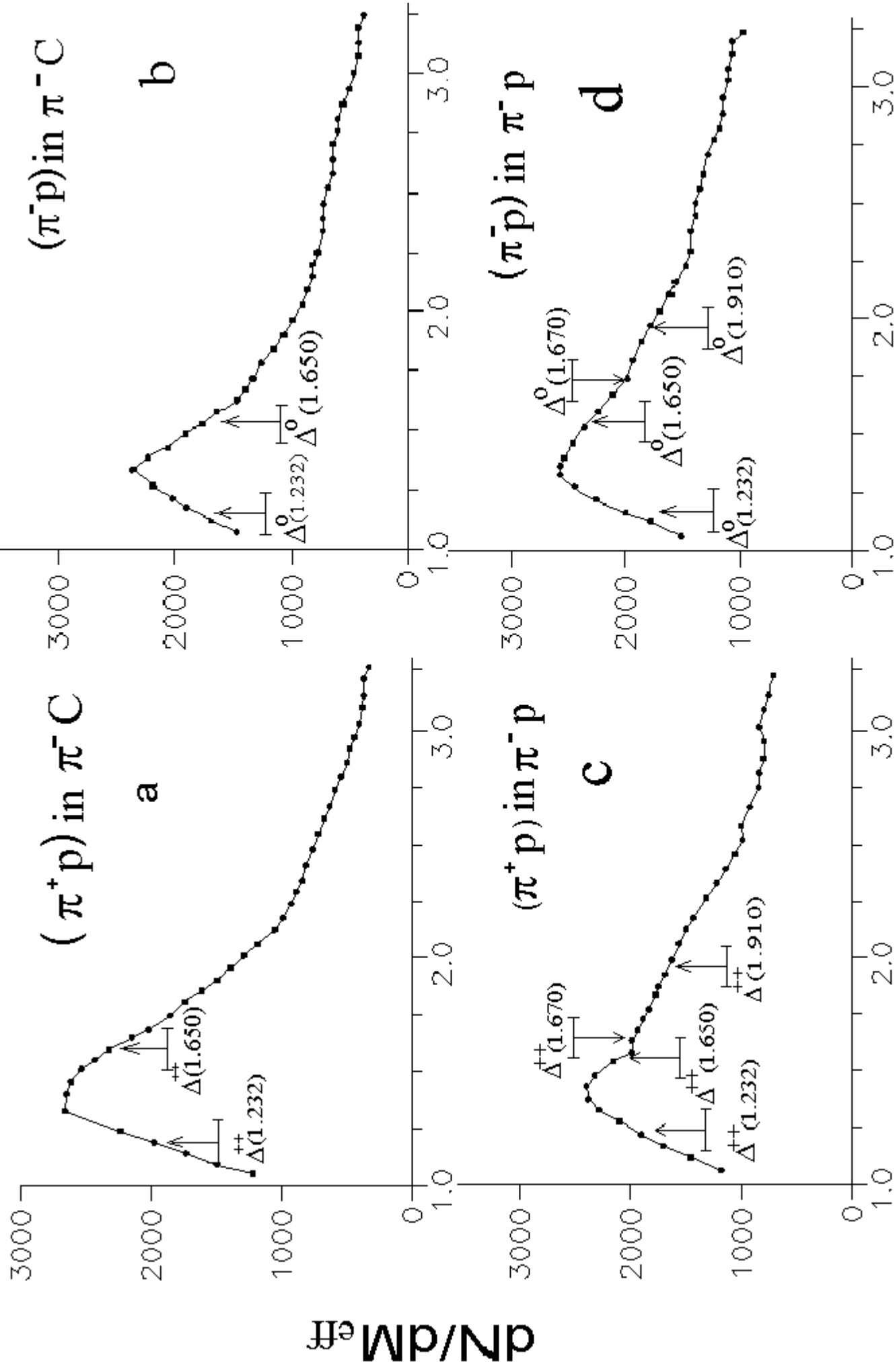
The authors wish to thank S. S. Shimansky for useful discussions.

## References

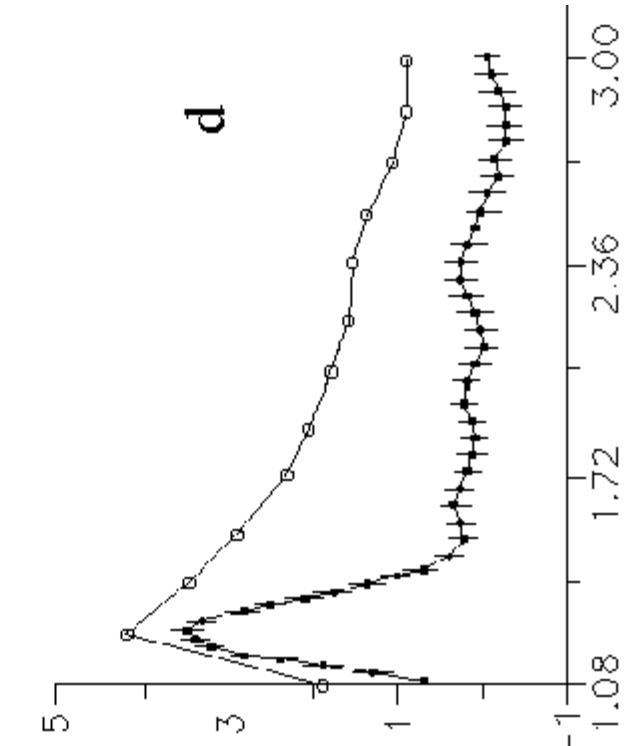
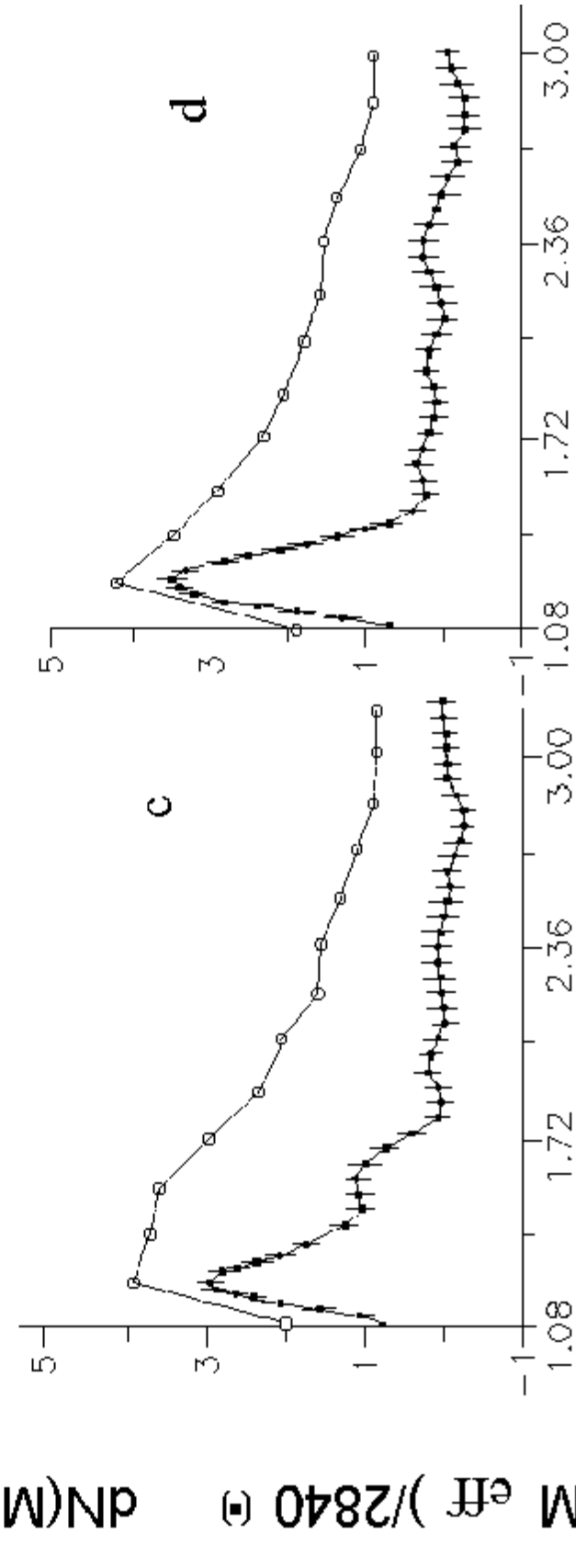
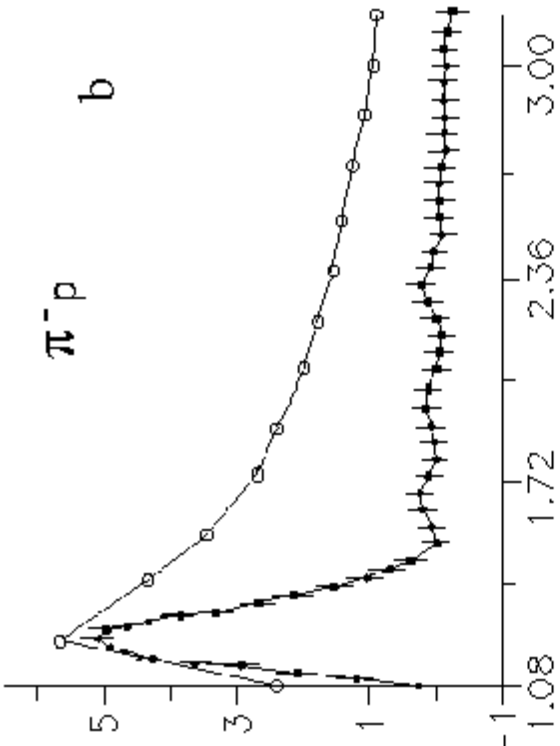
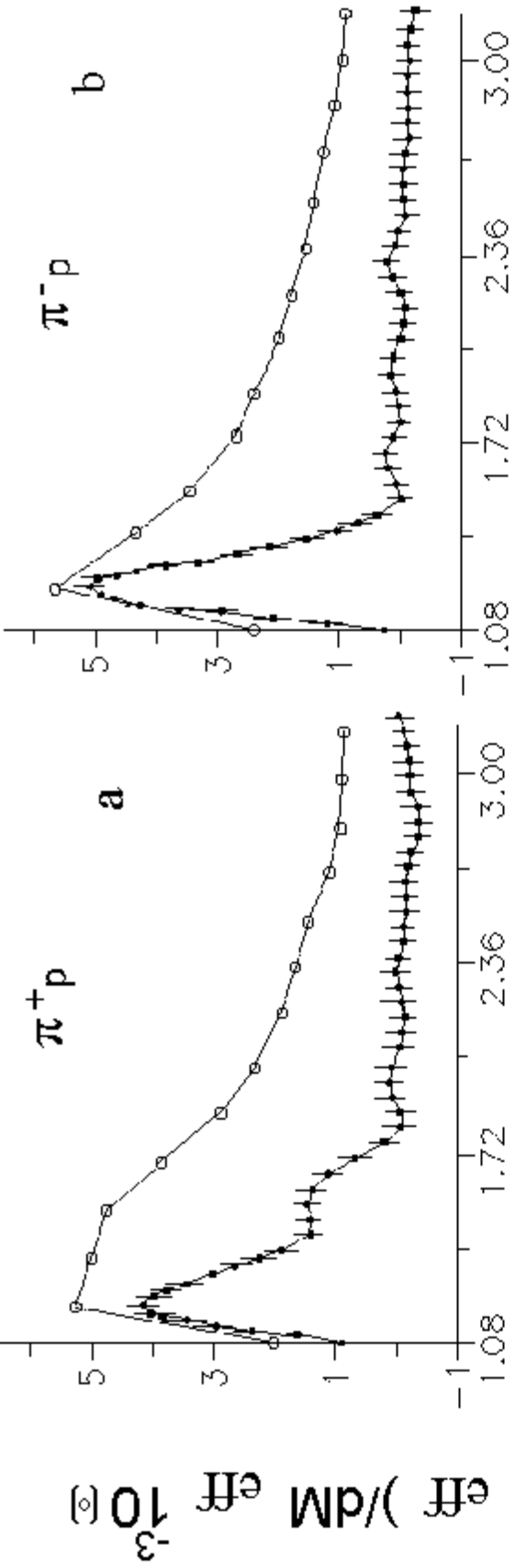
- [1] G. I. Kopylov and M. I. Podgoretsky. Function of a mutual coherence and multiple birth. *Sov.Nucl.Phys.*, 1974, 19, pp. 434-446.
- [2] B. Z. Belashev, M. K. Suleimanov and A. P. Cheplakov. Definition of spatial performances of process of multiple birth of particles. Preprint JINR, 1-80-150, Dubna, 1980.
- [3] A. I. Anoshin et al. Searching for barion resonances in effective mass spectra ( $\pi^\pm p$ ) pairs through the modified Fourier algorithm. Preprint JINR, 1-80-574, Dubna, 1980.
- [4] A. I. Anoshin et al. Analysis of the effective mass spectra ( $\pi^\pm p$ ) pairs in  $\pi^{-12}C$  interactions through Fourier algorithm. Report JINR, 1-81-680, Dubna, 1981.
- [5] A. I. Anoshin et al. Analysis of distributions of  $\pi$ -mesons on rapidity in reactions of  $\pi^- p$  and  $\pi^{-12}C$  interactions through Fourier algorithm. Report JINR, 1-81-68, Dubna, 1981.
- [6] A. I. Anoshin et al. Analysis of spectra containing resonances through Fourier algorithm. Report JINR, 1-81-679, Dubna, 1981.
- [7] B. Z. Belashev and A. N. Yakovlev. Application of maximum entropy for treatment of X-ray diagrams and the gamma spectra of amorphous minerals. *Trans. of RSNE'* 97, Dubna, 1997, v.1, pp. 92-94.
- [8] V. L. Aksenov and A. M. Balagurov. Neutron diffraction. *UFN*, 1996, 166, 9, pp. 955-985
- [9] J. Uo. *New ideas in NMR.* oscar, 1975.
- [10] B. Z. Belashev and L. M. Soroko. Data processing by the maximum entropy method. Report JINR, 10-80-696, Dubna, 1980.
- [11] B. Z. Belashev. Methods for reconstruction of diffuse spectra. *Jour. Appl. Spectr.*, 2001, 68, 5, pp.639-645.
- [12] A. I. Anoshin et al. The study of  $\pi^{-12}C$  interactions at  $P_{\pi^-} = 40$  GeV/c accompanied by emission of cumulative p-mesons. *Sov.Nucl.Phys.*, 1980, 31, 3, pp. 668-673.
- [13] G. S. Adams, T. Adams, Z. Bar-Yam et al. Observation of a New  $J = 1$  Exotic State in Reaction  $\pi p - \pi \pi \pi p$  at 18 GeV/c. *Phys. Rev. Lett.*, 81, 26, 1998, pp. 5760-5763.

## List of Figures

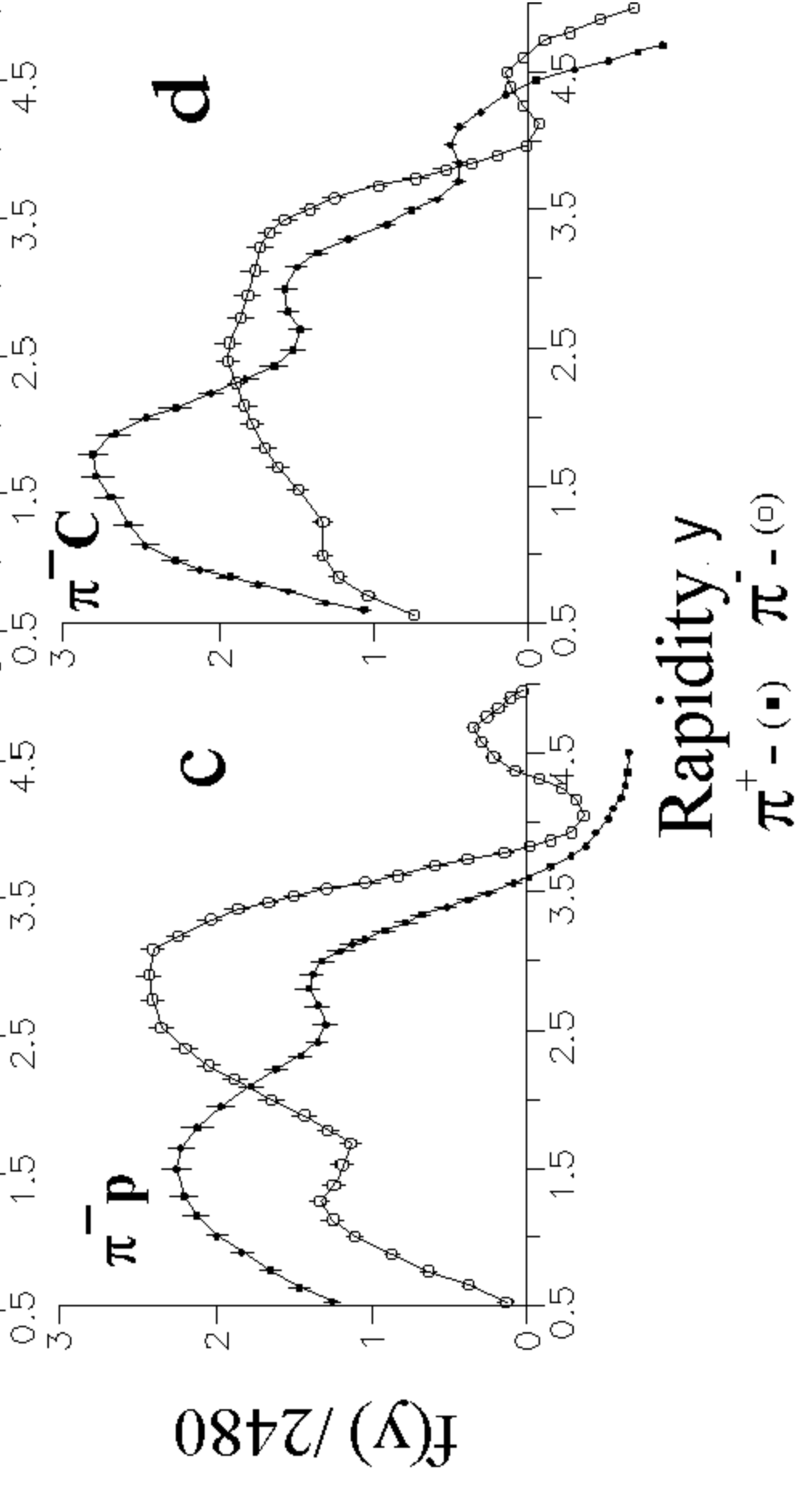
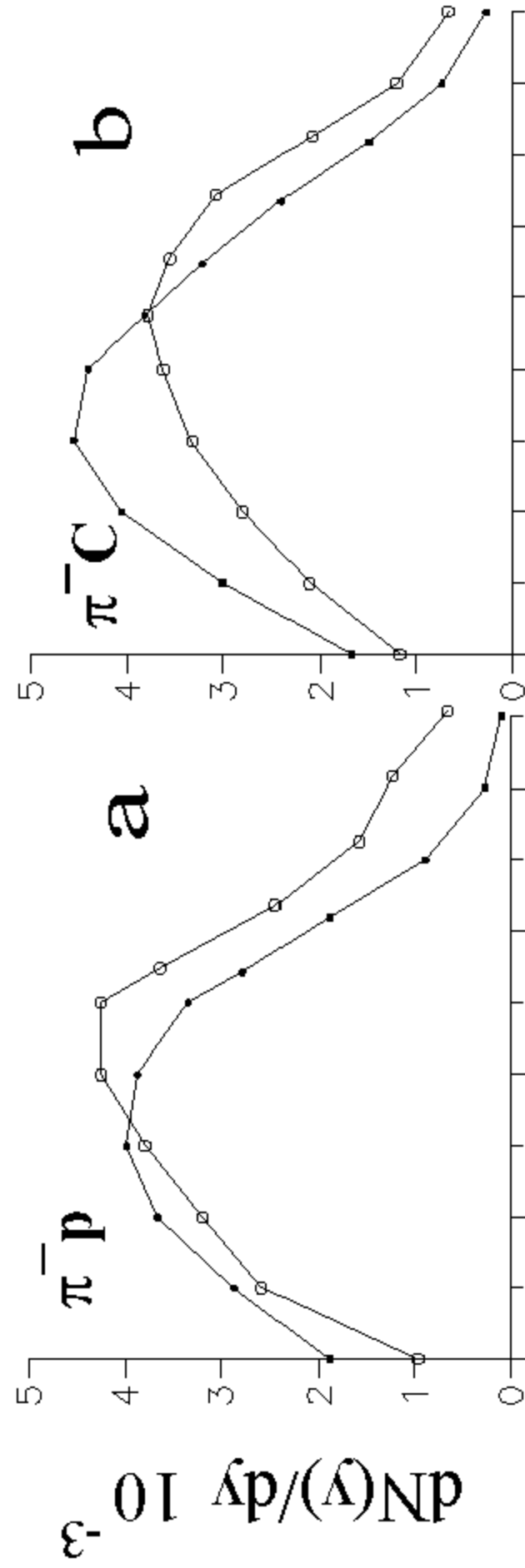
- Fig.1. Results of the application of the modified Fourier algorithm to effective mass spectra of  $(\pi^\pm p)$  pairs in  $\pi^-p$  and  $\pi^{-12}C$  interactions at  $P_{\pi^-} = 40$  GeV/c.
- Fig.2. Effective mass spectra  $dN(M_{eff})/dM_{eff}$  of  $(\pi^\pm p)$  pairs ( $\circ$ ), their estimation  $f(M_{eff})$  ( $\bullet$ ) for two schemes of selection of  $\pi$ -mesons.
- Fig.3. Rapidity-based distribution of  $\pi$ -mesons in  $\pi^-p$  (a) and  $\pi^{-12}C$  (b) interactions and their estimates (c) and (d), respectively, obtained with the help of Fourier algorithm used to control spectral line widths.
- Fig.4. Neutron diagram of a powder combination measured with a usual time flight diffractometer (a) and by Fourier diffractometer under high-resolution conditions on reactor IFR-2 (JINR, DUBNA) (b) and obtained as a result of MENT processing of the diagram (a): the MENT estimation and its touch-diagram (c).
- Fig.5. NMR spectrum  $^{13}C$  of adamantane recorded by the forced precession method (curve 1) and with the help  $\pi/2, \pi$ -sequence of impulses (curve 2) (a) and the MENT estimation of a curve 1 (curve 3) and its touch diagram (curve 4) (b).

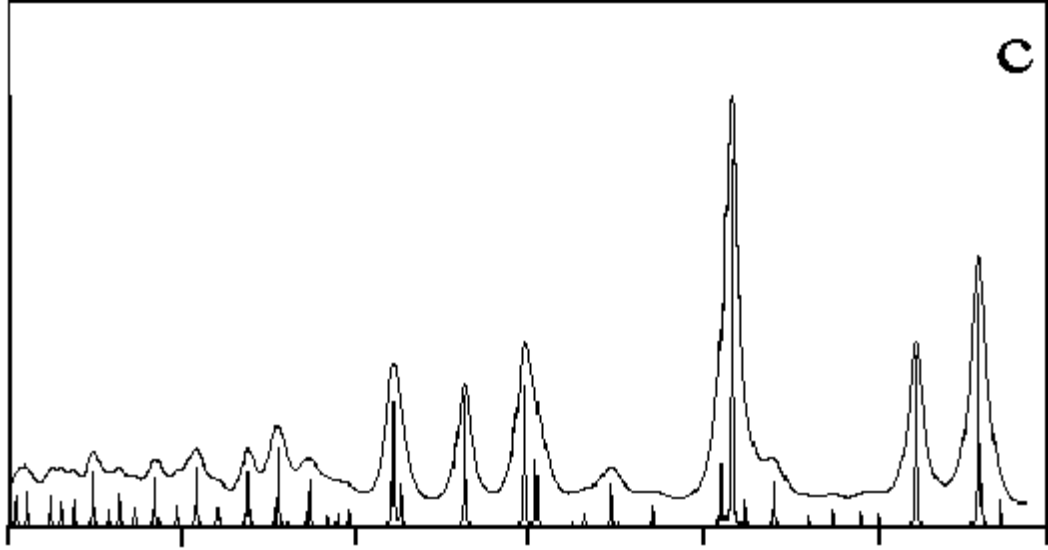
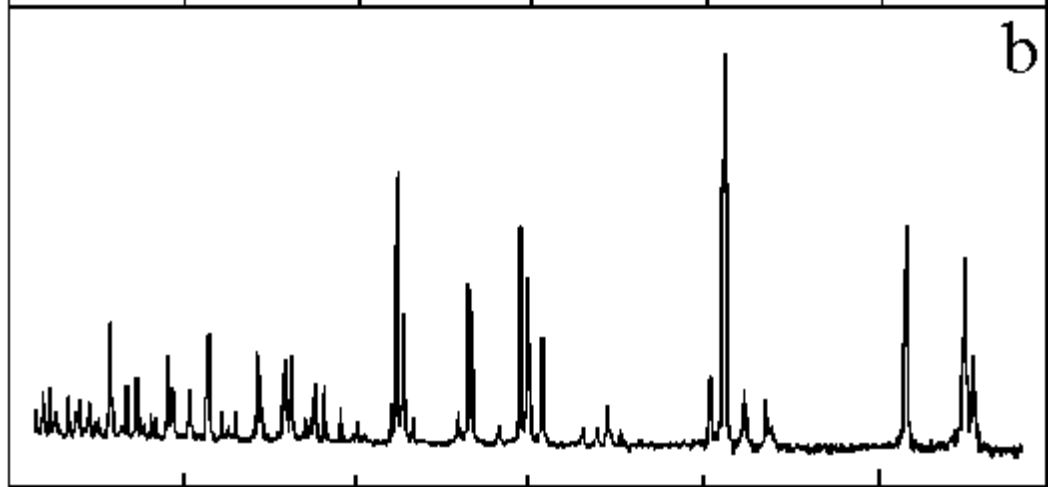
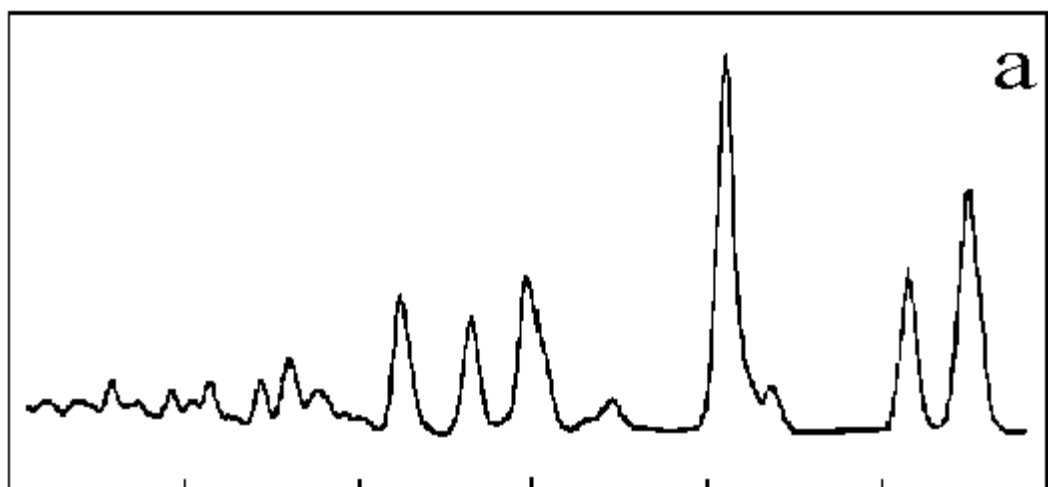


$M_{\text{eff}}$  GeV/c<sup>2</sup>



$M_{\text{eff}} \text{ (GeV}/c^2\text{)}$





0.7 1.0 1.3 1.6 1.9 2.2 2.5  
d, Å

